ICCCM-JOURNAL OF SOCIAL SCIENCES AND HUMANITIES
2026; 5 (sp): 123-130
Published online 3 25 2026 (https://icccmjssh.com/)
doi: https://doi.org/10.53797/icccmjssh.v5isp.14.2026
e-ISSN 2811-4469

Energy Regeneration and Dissipation in Electromagnetic and Magneto-Rheological Shock Absorbers Based on Vibration

Gad, A. S.[1] & Jabeen, S. D.[2]

[1]Delta Technological University, Industrial Zone, Quesina, Menoufia, EGYPT
[2]Department of Mathematics, Birla Institute of Technology Mesra, Ranchi 835215, INDIA

*Corresponding Author: ahmed01140938289@gmail.com

To Cite This Article:
Gad, A. S. & Jabeen, S. D. (2026). Energy Regeneration and Dissipation in Electromagnetic and Magneto-Rheological Shock Absorbers Based on Vibration. *ICCCM Journal of Social Sciences and Humanities*,5 Special Issue, 123-130. https://doi.org/10.53797/icccmjssh.v5isp.14.2026

Received 19 February 2026. **Revised** 25 February 2026, **Accepted** 13 March 2026, **Available online** 25 March 2026

Abstract: Electromagnetic and magnetorheological dampers have established significant in recent years due to their flexibility and efficiency as passive or semi-active damping devices, which require minimal power. Electromagnetic dampers can operate in four control modes: passive, semi-active, active, and hybrid, allowing them to meet various damping needs without the need for large power sources. Damping in electromagnetic systems can occur in two domains, either mechanical or electrical. In the mechanical domain, an electromagnetic damper typically includes components like a permanent-magnet DC motor, a ball screw and a nut. These components facilitate mechanical energy conversion, often analysed through energy regeneration and dissipation cases. In the electrical domain, the damper's core components coils and permanent magnets work together to generate electric energy, which varies based on control modes. In the fully passive mode within the electrical domain, the damper produces an electric load passively without external control. In the semi-active mode, a controlled voltage is applied to adjust the damping force dynamically based on road surface conditions, allowing the system to respond to changing demands for improved ride comfort. Adjusting the magnetic field strength directly influences damping characteristics, creating a roughly circular, nonlinear damping response as voltage increases. As a result, both damping force and power dissipation increase, peaking at the maximum damping rate, aligning with vehicle dynamics to enhance comfort and stability. These electromagnetic dampers demonstrate a promising approach to adaptive suspension systems, effectively balancing energy efficiency, ride comfort, and dynamic stability across different operating conditions.

Keywords: Electromagnetic damping systems, magnetorheological dampers, semi-active control, adaptive suspension systems, and energy regeneration.

1. Introduction

In traditional automotive suspension systems, passive components, such as fixed spring stiffness and damping coefficients, help absorb vibrations caused by road irregularities by dissipating the energy as heat. Each wheel's suspension unit typically involves a hydraulic shock absorber paired with a suspension spring. This design reduces vibrations by dissipating them as heat, effectively "wasting" the energy instead of repurposing it. However, regenerating this wasted energy has become an important goal in modern suspension systems, especially for hybrid and electric vehicles. Standard viscous shock absorbers, which rely on fluid resistance, are not well-suited for energy regeneration. To address this, electromagnetic and magneto-rheological (MR) dampers have emerged as alternatives. These devices are designed to convert dissipated vibration energy into electrical energy, which can be stored and reused, making them more energy-efficient and sustainable. The structure of electromagnetic dampers is such that can operate in either the mechanical or electrical domain. In the mechanical domain, the damper includes components like a permanent-magnet DC motor, ball screw, and nut. As the vehicle encounters road irregularities, these components work together to convert vibrational energy into rotational energy. This rotational energy is then transformed into electrical energy by the motor, allowing the damper to manage vibrations and generate usable power.

As proposed in El-Demerdash (2002), this approach optimizes the damper's performance and improves vehicle performance by generating energy from road-induced vibrations. By replacing traditional dampers with electromagnetic or MR dampers, automotive suspension systems can improve ride quality and capture lost energy that would otherwise

be wasted as heat. By using these technologies, automotive applications can shift from simple energy dissipation to energy regeneration, offering potential benefits for electric and hybrid vehicles by supporting auxiliary power systems. This advancement aligns with the push for sustainable energy solutions in automotive technology, improving ride quality and energy efficiency (El-Demerdash, 2002). The structure of a mechanical domain was changed modified into a permanent magnetic generator with a rack–pinion mechanism Ibrahim & El-Demerdash (1999), or alternatively into a system comprising a DC brushless motor, rack - pinion mechanism and rectifier circuit. These modifications were designed to evaluate the energy harvested and recover vibration energy effectively. adjusted by varying the resistance applied to the DC-brushless linear or rotate electric motors, which are connected to electric terminals and a resistive load (Soliman, 2016).

The Electrical domain of an electromagnetic damper comprises four key components: a permanent magnet array, a coil windings array, two guide cylinders and a spiral spring. The structure and operating principle of this domain were analysed in Zareh et al. (2012), focusing on the generation of regenerative electric power through the relative vertical motion between the coil and permanent magnet assemblies. Two configurations, linear and rotary devices, were selected as from electrical-domain shock absorbers to develop regenerative electric power (Ahn et al., 2009). Additionally, the electro-mechanical and thermal characteristics of these systems were investigated both numerically and experimentally providing valuable insights into their performance (Askari & Davaie-Markazi, 2008). Finite element methods and MATLAB software programmers were utilized to simulate and analyse the energy-harvested from shock absorber design (Wang, 2009). The numerical analysis was validated through experimentation. The efficiency of the developed electromagnetic vibration energy harvesting systems was thoroughly evaluated by (Zong et al., 2012). The passive electromagnetic damper cannot completely isolate the automobile body from road disturbances. Their low damping force, designed primarily for energy generation, results in restricted performance under fixed conditions and parameters. This limitation makes them less effective at handling dynamic road conditions. Semi-active control systems provide enhanced damping strategies, improving ride comfort and maintaining vehicle stability within acceptable limits for the automotive industries. They offer several advantages, including mechanical simplicity, high dynamic range, low power requirements, large force capacity, and robustness (Nugroho et al., 2014).

These systems combine the best features of both passive and active technologies, offering the reliability and fail-safety of passive devices while maintaining the adaptability and performance of fully active systems (Atray & Roschke, 2004). According to the aforementioned definitions, a semi-active control device has properties that can be adjusted in real time, ensuring optimal performance. Additionally, these devices are safer, as they can continue to function as passive systems if the control system fails. Semi-active control applications use four types of damping devices, electromagnetic dampers, viscous fluid dampers, tuned liquid dampers, and friction dampers. Among these, magnetorheological (MR) viscous fluid dampers and electromagnetic shock absorbers have gained significant popularity in automobile suspension systems, owing to their adaptability and ability to enhance ride comfort and vehicle stability. MR viscous fluid shock absorbers exhibit performance comparable to fully active suspension systems in enhancing ride comfort while being more cost-effective.

The ride comfort directly correlates with the voltage applied to the MR damper, meaning that an increase in voltage enhances damping performance. However, this improvement comes at the cost of higher power consumption, which remains a topic of debate among researchers in this field. A novel MR damper with a multistage piston and independent input currents was designed and analysed to optimize energy recycling (Choi et al., 2002). Research has also examined the energy balance between MR dampers and vibration reduction systems (Tseng & Hrovat, 2015). Additionally, compact power generation mechanisms in parallel with MR dampers Marzbanrad et al. (2004), and MR dampers connected to an electromechanical transducer Roh & Park (1998), were used to recycle the energy of dissipated into the system. Two magnetic fields are induced inside the MR damper, one is in the outer coil of the power generator and another in the piston head coils Youn et al. (2017) to evaluate the ability of generating energy. The electromagnetic damper, functioning as semi-active tubular machine Gad (2021), represents a novel that does not use permanent magnets. Instead, it relies solely on windings on both the translator and the stator. The translator coil is connected to an external direct-current (DC) source, in which the generated magnetic flux density can be controlled by tuning the amount of DC current supplied. A Tubular electromagnetic actuator, designed for semi-active suspension, consists of permanent magnets, 3-phase coils, stator iron, and translator back-iron, it was as suggested by (Shehata, 2023).

The novel contributions of this paper include the estimation of both dissipative and regenerative power for three different damper types: the mechanical domain of a passive electromagnetic damper, the electrical domain of an electromagnetic damper (both passive and semi-active), and magneto-rheological (MR) damper (both passive and semi-active). In the electrical domain of the electromagnetic damper a passive controller is converted into a semi-active controller. After that, the dissipation powers of electrical domain and magneto-rheological dampers in their semi-active configurations are compared to identify which provides superior performance with minimal power consumption. Additionally, the regenerative powers of all proposed dampers are evaluated to determine which configuration delivers the highest electrical power output. The rest of this article is organized as follows: The study begins by examining two cases of the mechanical domain: dissipation and regeneration modes. Subsequently, the electrical domain is analysed, focusing on the conversion from a passive controller to a semi-active controller, accompanied by a comparative

evaluation of dissipation power. Finally, regeneration power is evaluated based on the working capacity of the proposed dampers

2. Mechanical Domain of Passive Electromagnetic Damper

The mechanical domain of an electromagnetic damper is modeled as a passive damper, utilizing components such as a permanent-magnet DC motor, a ball screw, and a nut, as illustrated in Figure 1.

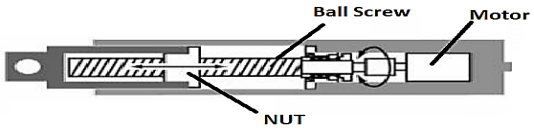

Figure1. Passive Mechanical Domain of an Electromagnetic Damper.

The corresponding output force F is defined as follows:

$$F = U - C_e\dot{X}_{bw} - I\,\ddot{X}_{bw}\,;$$

$$\text{Where}\begin{cases} U = -\emptyset\, i, \\ \emptyset = \frac{2\pi}{L} k_m, \\ i = \frac{\emptyset}{R}\dot{X}_{bw}, \\ I = \left(\frac{2\pi}{L}\right)^2 (J_m + J_b). \end{cases} \quad (1)$$

The force (U), equivalent inertia (I), equivalent damper coefficient (Ce), motor constant (Φ), current (i), ball screw lead (L), and total resistance (R), which includes both internal resistance of the motor and any added resistance placed in the circuit. The EDMD can operate in two different methods either dissipation mode or regeneration mode. When the magnitude of the converted factor is less than the condenser voltage, the electromagnetic damper is operates in dissipation mode. Conversely, when the magnitude of the converted factor exceeds the condenser voltage, the damper operates in regeneration mode converting vibration energy into usable power. The equations describe describing the dissipation and regeneration modes of the EDMD are listed as follows:

Case (1): Regeneration Mode

$$When\ \emptyset|\dot{X}_{bw}| \geq E$$

$$F_{regeneration} = U - C_e\dot{X}_{bw} - I\,\ddot{X}_{bw}\,;$$

$$Where\begin{cases} U = -\frac{\emptyset^2}{R}\dot{X}_{bw} + \frac{\emptyset}{R} E\ sign\left(\dot{X}_{bw}\right), \\ i = \frac{\emptyset|\dot{X}_{bw}| - E}{R}, \\ \dot{E} = \frac{1}{C_{Condenser}}\left(\frac{\emptyset|\dot{X}_{bw}| - E}{R}\right). \end{cases} \quad (2)$$

Figure 2(a) shows the relationship between time and the suggested ground velocity, while Figure 2(b) depicts the relationship between time and the factor describing the converted voltage. Figure 2(c) presents the relationship between time and condenser voltage, highlighting that an increase in condenser capacity leads to a decrease in converted voltage. Lastly, Figure 2(d) illustrates the relationship between time and the converted force of a dissipation mode to a regeneration mode. It is observed that the converted force depends directly on the condenser capacity, and the spent time required to convert this force increases when the capacity of a condenser increases. Figure.2 (c) and Figure.2 (d) are plotted for condenser capacities of 5F, 10F, and 15F.

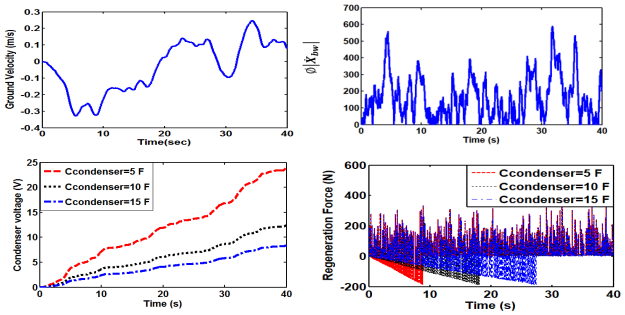

Figure 2. Effect of road excitation frequency on the power regeneration from an EDMD

Case (2): Dissipation Mode

$$\text{When } \emptyset\left|\dot{\mathbf{X}}_{\mathbf{bw}}\right| \leq \mathbf{E}$$

$$\mathbf{F_{dissipation}} = \mathbf{U} - \mathbf{C_e}\dot{\mathbf{X}}_{\mathbf{bw}} - \mathbf{I}\,\ddot{\mathbf{X}}_{\mathbf{bw}}\,,$$

$$\text{Where } \begin{cases} \mathbf{U} = -\frac{\emptyset^2}{\mathbf{R}}\dot{\mathbf{X}}_{\mathbf{bw}}, \\ \dot{\mathbf{E}} = \mathbf{0}. \end{cases}$$

Here, $\emptyset\left|\dot{X}_{bw}\right|$ represents the rate of the converted voltage, E is the condenser voltage, and $C_{Condenser}$ is the capacity of the condenser.

Figure 3 illustrates the dissipation mode characteristic curve of the EDMD. The relationship between displacement, velocity and force loop indicates that, the force occurs approximately between -1500 N and 1500 N. and This range reflects an increase in the quantity of dissipation energy, which positively impacts ride comfort and dynamic stability because the damping rate increasing significantly. In contrast, Figure 2 shows that the regeneration force occurs between -200N and 200N, resulting in a limited damping rate. Consequently, the ride comfort and dynamic stability provided by regeneration are minimal compared to damping rate achieved due to regeneration case.

(3)

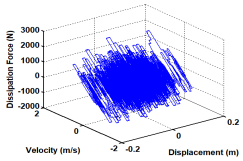

Figure3. Illustration of the dissipation Mode Characteristic Curve of the EDMD

3. Electrical Domain of an Electromagnetic Damper

The electromagnetic damper can operate in three different modes: fully passive, semi-active and active. Additionally, the force-velocity relationship can be adjusted by altering the electric load connected to the device. The semi-active mode is the most effective to connect the electric load to achieve optimal ride comfort and dynamic stability, but it requires an electric power supply. Conversely, in the passive mode, the device generates electric power but compromises on ride comfort and dynamic stability. The classifications for both fully passive and semi-active modes of this device are listed as follows:

3.1 Generation of Electric Load by Fully Passive Electromagnetic Dampers

A passive electromagnetic damper (Electrical Domain) consists of two key components: a permanent magnet array, which is connected to the vehicle's wheel axles and a coil windings array, which is fixed to the vehicle's framework. These components are separated by an when the vehicle moves over rough terrain, the relative displacement between the sprung mass (the vehicle body) and the unsprung mass (the wheels and axles) causes the coil array to move relative to the permanent magnets. This motion induces a current in the coils as they cut through the magnetic induction lines within the air-gap. This current generates a damping force that opposes the motion of the vehicle. The structure of the damper is similar to that described in reference Zareh et al. (2012), as illustrated in Figure 4. This interaction results in a magnetic damping force that aids in controlling the suspension system's motion, improving ride comfort and vehicle stability. This induced current generates a damping force, which acts in the opposite direction of the coil's movement. The total damping force is determined by two primary factors: the Magnetic Damping Force, which arise from the interaction between the induced current in the coils and the magnetic field, and, the Inertial Force, which results from the motion of the coil relative to the permanent magnet array. The gravity of the coil is neglected in this study to simplify the model. The overall damping force exerted by the electromagnetic damper is described as:

$$\boldsymbol{F = F_i + F_d = m_{coil}\left(\frac{dx}{dt}\right)^2 + \gamma\frac{dx}{dt} = m_{coil} \times a}$$

(4)

$$\boldsymbol{F_d = \sigma\ \frac{dx}{dt}\ B_r^2\ V_{coil} = \gamma\frac{dx}{dt}}$$

(5)

The inner and outer radial magnetic flux densities in coils array are:

$$\boldsymbol{B_{ri} = \frac{V_{ei}}{\frac{dx}{dt}Li} = \frac{V_{ei}}{\frac{dx}{dt}\pi\, N\, D_{r1}}, and\ \ B_{ro} = \frac{V_{eo}}{\frac{dx}{dt}Lo} = \frac{V_{eo}}{\frac{dx}{dt}\pi\, N\, D_{r2}}}$$

(6)

So, the total radial magnetic flux is,

$$\boldsymbol{B_r = B_{ri} + B_{ro} = \frac{V_{ei}}{\frac{dx}{dt}\pi\, N\, D_{r1}} + \frac{V_{eo}}{\frac{dx}{dt}\pi\, N\, D_{r2}}}$$

(7)

The conductivity is 5×10^7 s/m, the turns of the single coil array is 40, and the volume of coil array is

$$\boldsymbol{V_{coil} = V_{coil}(inner) + V_{coil}(outer) = \pi(R_4^2 - R_3^2)h_5 + \pi(R_6^2 - R_5^2)h_5} \quad (8)$$

The inner and outer electric conductivities of coils are:

$$\boldsymbol{\sigma_i = \frac{N\,\pi\,D_{r1}}{R_c\,A_{w1}} and\ \sigma_o = \frac{N\,\pi\,D_{r2}}{R_c\,A_{w2}}} \quad (9a)$$

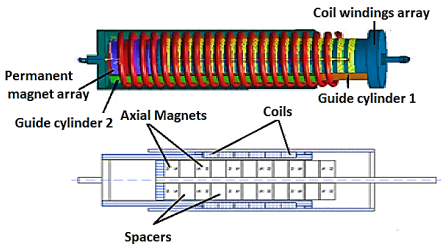

Figure 4. A passive electromagnetic damper

By substituting Equations (6) to (9) in Equation (5), the damping force becomes:

$$\boldsymbol{F_d = F_{di} + F_{do} = \frac{N\,\pi\,D_{r1}}{R_c\,A_{w1}} \times \frac{dx}{dt} \times \left(\frac{V_{ei}}{\frac{dx}{dt}\pi\,N\,D_{r1}}\right)^2 \times \pi(R_4^2 - R_3^2)h_5 + \frac{N\,\pi\,D_{r2}}{R_c\,A_{w2}} \times \frac{dx}{dt} \times \left(\frac{V_{eo}}{\frac{dx}{dt}\pi\,N\,D_{r2}}\right)^2 \times \pi(R_6^2 - R_5^2)h_5} \quad (10)$$

The total regenerated power of an electromagnetic damper for passive case is,

$$\boldsymbol{P_{reg} = \frac{((\frac{dx}{dt})_{max}\,B_r)^2 \sigma\,V_{coil}}{12}} \quad (11)$$

Here: $\boldsymbol{F}$ is the force of an electromagnetic damper (N), which comprises two components: $\boldsymbol{F_i}$ is the inertial force, and, $\boldsymbol{F_d}$ the magnetic damping force. The relative velocity between the sprung and un-sprung masses is denoted by $\frac{dx}{dt}$ (m/s), $\boldsymbol{a}$ is the acceleration of coil array (m/s2), $\boldsymbol{\gamma}$ is the damping coefficient, Br is the radial magnetic flux density, $\boldsymbol{\sigma}$ is the electric conductivity of the coil, $\boldsymbol{V_{coil}}$ is the total volume of coil array (m³), $\boldsymbol{V_{ei}}$ is the inner induced electromotive force (V), and $\mathbf{V_{eo}}$ is the outer induced electromotive force (V). Table 1 illustrates the geometric dimensions used in passive electromagnetic damper proposed in this study.

Figure 6 demonstrates the characteristic curves of a passive electromagnetic damper model. The curves are derived based on an input displacement described by x = A sin (2πt), where the amplitude A is set to 7 cm. These curves are plotted for a circuit operating without load current and include five distinct graphs. Each graph offers insights into the dynamic behaviour of the damper, providing a comprehensive representation of its response to the input displacement. The relationships depicted in Figure 6 are as follows: Figure 5(a) shows the force versus velocity relationship, which captures the dynamic interaction between the damping force and the relative velocity of the damper. Figure 5(b) illustrates the force versus displacement relationship, highlighting how the damping force varies with the displacement of the system. Figure 5(c) demonstrates the force versus time relationship, displaying how the damping force changes over time. Figure 5(d) presents a loop of displacement and velocity versus force, providing a comprehensive visualization of the correlation between displacement, velocity, and force within the damper system.

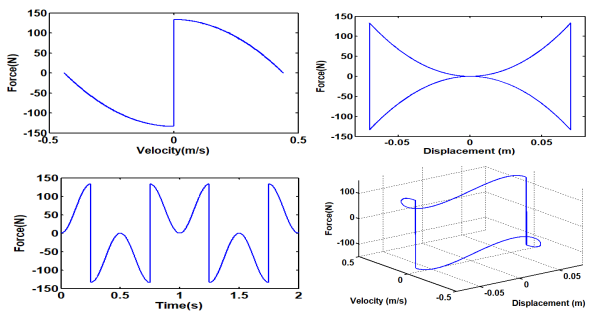

Figure 5. Characteristic curves of a passive electromagnetic damper model

3.2 Semi-Active Case, if the Electromagnetic Damper Requiring Variables Electric Load

In the semi-active case of an electromagnetic damper, the differential eddy current dI passing through a differential cross section area of the coil winding is given by:

$$dI = J\ dA_w \tag{11}$$

where J represents the current density and Aw is the area of the cross-section of the coil winding (m²).
By integrating the dI over the cross section, the total eddy current I of the coil (A) is obtained:

$$I = \sigma\ B_r\ A_w \frac{dx}{dt} \tag{12}$$

The relationship between the current (I) passing through a differential cross section area of the coil winding and the damping force depends on how the coils are connected to the external circuit. Therefore, the current applied to the inner and outer coils arrays from the external circuit will be:

$$\left[L_{coil}\frac{dI_i}{dt} + (R_{coil} + R_{load})\ I_i\right] + \left[L_{coil}\frac{dI_o}{dt} + (R_{coil} + R_{load})\ I_o\right] = \frac{N\,\pi\,D_{r1}}{R_c\,A_{w1}} \times \frac{dx}{dt} \times \left(\frac{V_{ei}}{\frac{dx}{dt}\pi\,N\,D_{r1}}\right)^2 \times \pi(R_4^2 - R_3^2)h_5 + \frac{N\,\pi\,D_{r2}}{R_c\,A_{w2}} \times \frac{dx}{dt} \times \left(\frac{V_{eo}}{\frac{dx}{dt}\pi\,N\,D_{r2}}\right)^2 \times \pi(R_6^2 - R_5^2)h_5 \tag{13}$$

Equation (13) describes the relationship between the total damping force generated by of an electromagnetic damper in the semi-active case and the current applied to the inner and outer coil arrays from the external circuit. The damping force is changed according to applied current in the inner and outer coil arrays, and is given by the following expression:

$$F_d = F_{di} + F_{do} = \frac{N\,\pi\,D_{r1}}{(R_{coil}+R_{load})\,A_{w1}} \times \frac{dx}{dt} \times \left(\frac{L_{coil}\frac{dI_i}{dt} + (R_{coil}+R_{load})\,I_i}{\frac{dx}{dt}\pi\,N\,D_{r1}}\right)^2 \times \pi(R_4^2 - R_3^2)h_5 + \frac{N\,\pi\,D_{r2}}{(R_{coil}+R_{load})\,A_{w2}} \times \frac{dx}{dt} \times \left(\frac{L_{coil}\frac{dI_o}{dt} + (R_{coil}+R_{load})\,I_o}{\frac{dx}{dt}\pi\,N\,D_{r2}}\right)^2 \times \pi(R_6^2 - R_5^2)h_5 \tag{14}$$

In this equation, the damping force is determined by the contributions from both the inner and outer coils, with each coil's behaviour influenced by the external circuit's applied current. The forces depend on factors such as coil resistance, inductance, and geometry, as well as the applied velocity and displacement of the system. The performance of an electromagnetic damper as a semi- active device is described by two operational modes (cases): one is regeneration mode, where the applied current to the device is turned off. As a result, the damper operates without external control, generating electric power from the relative motion between the coil and magnet array. This case is illustrated in Figure 5. The other controllable mode (semi-active mode), in which the applied current is controlled by external units to vary the damping force based on the vehicle's dynamic conditions. This adaptability allows the damper to adjust its behaviour for optimal performance, improving vehicle stability and ride comfort. The current is actively regulated to match the changing conditions, providing dynamic and responsive damping.

Figure 6 demonstrations the block diagram of a semi-active vibration control system using an electromagnetic damper. It involves of two nested controllers; a system controller and Power Electronics. The system controller utilizes the dynamic responses of the vehicle's behavior such as displacement, velocity, and acceleration to evaluate the desired damping force (FDesired) using specific control algorithms. These algorithms generally follow one of two approaches.The first is direct optimization techniques, like H∞ control or Linear-Quadratic-Gaussian (LQG) control, which optimizes state variables. The second is behaviour emulation, where models like Skyhook or sliding mode control mimic ideal system behaviours to improve the system's response and efficiency. So, it is important to determine the command current accurately to achieve the desired damping force (FDesired) in practical applications. The system can automatically switch the current according to the error between the parameters describing the damping rate and the desired damping force, depending on whether this error exceeds a set threshold. Power electronics play a crucial role in adjusting the current applied to the electromagnetic damper under the following conditions:

$$\textbf{switch} = \begin{cases} IF\ \left[L_{coil}\dfrac{dI_i}{dt} + (R_{coil}+R_{load})\,I_i\right] + \left[L_{coil}\dfrac{dI_o}{dt} + (R_{coil}+R_{load})\,I_o\right] \geq F_{\text{Desired}} \\ then\ I_i + I_o = \max\ (Dissipation\ mode\ of\ semi-active\ case) \\ IF\ \left[L_{coil}\dfrac{dI_i}{dt} + (R_{coil}+R_{load})\,I_i\right] + \left[L_{coil}\dfrac{dI_o}{dt} + (R_{coil}+R_{load})\,I_o\right] = F_{\text{Desired}} \\ then\ I_i + I_o = zero\ (\text{Regeneration } mode\ of\ a\ passive\ case) \\ IF\ \left[L_{coil}\dfrac{dI_i}{dt} + (R_{coil}+R_{load})\,I_i\right] + \left[L_{coil}\dfrac{dI_o}{dt} + (R_{coil}+R_{load})\,I_o\right] \leq F_{\text{Desired}} \\ then\ I_i + I_o = \max\ (Dissipation\ mode\ of\ semi-active\ case) \end{cases} \tag{15}$$

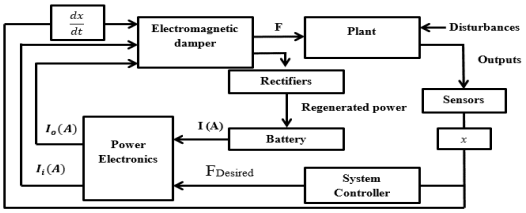

Figure 6. Block diagram of a semi-active control system for a plant integrated with an electromagnetic damper

Figure 7 illustrates the dissipation mode characteristic curves of an electromagnetic damper in a semi-active Case. The figure includes several relationships: Figure 7 (b) between displacement and dissipation force, Figure 7 (c) between time and dissipation force, and Figure 9 (d) a loop between displacement (m), velocity (m/s), vs. dissipation Force (N) According to these graphs, the response of the electromagnetic damper is evaluated for a 2.5 Hz sinusoidal input with an amplitude of 7cm, at five constant current levels; 0.5A, 1 A, 1.5A, 2A, and 2.5 A. The effects of changing the magnetic field are readily observed. As the voltage increases, the electromagnetic damper characteristics become approximately elliptical and nonlinear. This indicates that the damping force is more closely aligned with the vehicle's behavior, contributing to enhanced ride comfort and dynamic stability. However, the dissipation power also increases, reaching its maximum rate at the highest damping force.

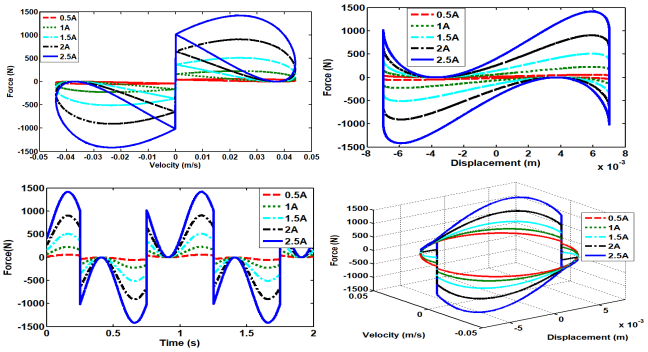

Figure 7. Characteristic curves of a semi-active

4. Conclusion

In conclusion, electromagnetic dampers, in both passive and semi-active modes, exhibit considerable potential for enhancing vehicle suspension systems. As outlined earlier, in the passive mode, damping forces arise from the interaction between the permanent magnets and the coil windings, which are influenced by the relative displacement between the sprung and unsprung masses during vehicle movement. This provides effective vibration suppression. In the semi-active mode, as the current supplied to the system is dynamically controlled, the damper's response is optimized, allowing for real-time adjustment of the damping force to match the vehicle's dynamic conditions. This mode enables the damper to switch between two operational modes: regeneration mode (current turned off) and controllable mode (current varied for desired damping force). The adjustable current in the coils significantly impacts the damping force, shifting the damper's behaviour from linear to nonlinear characteristics as the current increases, improving the ride quality and dynamic stability. However, this comes at the cost of higher dissipation power as the damping rate reaches its maximum. These findings highlight the effectiveness of electromagnetic dampers in achieving an ideal balance of ride comfort and vehicle stability, thus contributing to improved vehicle dynamics, especially in demanding road conditions.

Acknowledgement

The authors would like to thank the fellow authors and organizations whose intellectual properties were utilized for this study.

Conflict of Interest

The authors declare no conflicts of interest

References

Ahn, K. K., Truong, D. Q., & Islam, M. A. (2009). Modeling of a magneto-rheological (MR) fluid damper using a self tuning fuzzy mechanism. Journal of Mechanical Science and Technology, 23(5), 1485-1499. https://doi.org/10.1007/s12206-009-0359-7

Askari, M., & Davaie-Markazi, A. H. (2008, July). Multi-objective optimal fuzzy logic controller for nonlinear building-MR damper system. In 2008 5th International Multi-Conference on Systems, Signals and Devices (pp. 1-6). IEEE. https://doi.org/10.1109/SSD.2008.4632880

Atray, V. S., & Roschke, P. N. (2004). Neuro‐fuzzy control of railcar vibrations using semiactive dampers. Computer‐Aided Civil and Infrastructure Engineering, 19(2), 81-92. https://doi.org/10.1111/j.1467-8667.2004.00339.x

Choi, S. B., Lee, H. S., & Park, Y. P. (2002). H8 control performance of a full-vehicle suspension featuring magnetorheological dampers. Vehicle System Dynamics, 38(5), 341-360. https://doi.org/10.1076/vesd.38.5.341.8283

El-Demerdash, S. M. (2002, November). Improvement of Trucks Ride Dynamics Using a Hydraulic Semi-Active Suspension System. In International Truck & Bus Meeting & Exhibition. SAE Technical Paper. https://doi.org/10.4271/2002-01-3039

Gad, A. S. (2021). A preview type-2 fuzzy controller design for the semi-active suspension to improve adhesion characteristics during braking and handling (No. 2021-01-5069). SAE Technical Paper. https://doi.org/10.4271/2021-01-5069

Ibrahim, I. M., & El-Demerdash, S. M. (1999). Investigation of wheeled tractors ride comfort using hydraulic semi-active suspension system (No. 1999-01-3727). SAE Technical Paper. https://doi.org/10.4271/1999-01-3727

Marzbanrad, J., Ahmadi, G., Zohoor, H., & Hojjat, Y. (2004). Stochastic optimal preview control of a vehicle suspension. Journal of sound and vibration, 275(3-5), 973-990. https://doi.org/10.1016/S0022-460X(03)00812-5

Nugroho, P. W., Li, W., Du, H., Alici, G., & Yang, J. (2014). An adaptive neuro fuzzy hybrid control strategy for a semiactive suspension with magneto rheological damper. Advances in Mechanical Engineering, 6, 487312. https://doi.org/10.1155/2014/487312

Roh, H. S., & Park, Y. (1998). Observer-based wheelbase preview control of active vehicle suspensions. KSME International Journal, 12(5), 782-791. https://doi.org/10.1007/BF02945545

Shehata Gad, A. (2023). Interval Lower Singleton Fuzzy Optimal Controller Design of Magnetorheological Seat Suspension Integrated with Semi-Active Vehicle Suspension System (No. 2023-01-5066). https://doi.org/10.4271/2023-01-5066

Soliman, A. M. (2016, April). Improvement of vehicle ride comfort using control strategies for the switchable damper suspension system. In SAE 2016 World Congress and Exhibition. SAE Technical Paper. https://doi.org/10.4271/2016-01-0441

Tseng, H. E., & Hrovat, D. (2015). State of the art survey: active and semi-active suspension control. Vehicle system dynamics, 53(7), 1034-1062. https://doi.org/10.1080/00423114.2015.1037313

Wang, H. (2009). Modeling of magnetorheological damper using neuro-fuzzy system. In Fuzzy Information and Engineering Volume 2 (pp. 1157-1164). Berlin, Heidelberg: Springer Berlin Heidelberg. https://doi.org/10.1007/978-3-642-03664-4_123

Youn, I., Khan, M. A., Uddin, N., Youn, E., & Tomizuka, M. (2017). Road disturbance estimation for the optimal preview control of an active suspension systems based on tracked vehicle model. International Journal of Automotive Technology, 18(2), 307-316. https://doi.org/10.1007/s12239-017-0031-7

Zareh, S. H., Abbasi, M., Mahdavi, H., & Osgouie, K. G. (2012). Semi-active vibration control of an eleven degrees of freedom suspension system using neuro inverse model of magnetorheological dampers. Journal of Mechanical Science and Technology, 26(8), 2459-2467. https://doi.org/10.1007/s12206-012-0628-8

Zong, L. H., Gong, X. L., Guo, C. Y., & Xuan, S. H. (2012). Inverse neuro-fuzzy MR damper model and its application in vibration control of vehicle suspension system. Vehicle system dynamics, 50(7), 1025-1041. https://doi.org/10.1080/00423114.2011.645489